ADVANCES IN ATMOSPHERIC SCIENCES, VOL. 25, NO. 1, 2008, 126–138

Projected Potential Vegetation Change in China under the SRES A2 and B2 Scenarios

JIANG Dabang* (姜大膀)

Nansen-Zhu International Research Center, Institute of Atmospheric Physics, Chinese Academy of Sciences, Beijing 100029

(Received 9 January 2007; revised 29 March 2007)

ABSTRACT

The ability of seven global coupled ocean-atmosphere models to reproduce East Asian monthly surface temperature and precipitation climatologies during 1961–1990 is evaluated. January and July climate differences during the 2050s and 2090s relative to 1961–1990 projected by the seven-model ensemble under the Special Report on Emission Scenarios (SRES) A2 and B2 scenarios are then briefly discussed. These projections, together with the corresponding atmospheric CO_2 concentrations under the SRES A2 and B2 scenarios, are subsequently used to drive the biome model BIOME3 to simulate potential vegetation distribution in China during the 2050s and 2090s. It is revealed that potential vegetation belts during the 2050s shift northward greatly in central and eastern China compared to those during 1961–1990. In contrast, potential vegetation change is slight in western China on the whole. The spatial pattern of potential vegetation during the 2090s is generally similar to that during the 2050s, but the range of potential vegetation change against 1961–1990 is more extensive during the 2090s than the 2050s, particularly in western China. Additionally, there exists model-dependent uncertainty of potential vegetation change under the SRES A2 scenario during the 2090s, which is due to the scatter of projected climate change by the models. The projected change in potential vegetation under the SRES A2 scenario during the 2090s is attributable to surface temperature change south of 35°N and to the joint changes of surface temperature, precipitation, and atmospheric CO_2 concentration north of 35°N.

Key words: climate change, potential vegetation, projection, uncertainty

DOI: 10.1007/s00376-008-0126-1

1. Introduction

Climate change greatly affects agricultural harvests, energy supplies, and water resources and are directly related to economic and social sustainable development throughout the world. At present, climatology has become one of the most active branches in the geosciences. In recent decades, anthropogenic influences on climate system have been gradually intensified following industrial expansion and have received more and more attention worldwide, for instance through the well known and human-induced global warming. It has been shown that globally-averaged surface temperature has risen continually since 1861, and that during the 20th century this increment was (0.6±0.2)°C. Moreover, there is new and stronger evidence that most of the warming observed in the second half of the 20th century is attributable to human activities (IPCC, 2001).

The perspective of surface temperature warming in China in recent decades has been widely recognized. Moreover, the impact upon society has been notable, with generally negative effects on the national economy (Qin, 2003). At present, most scientists are engaged in the projection of climate change in inland China, using state-of-the-art climate system models driven primarily by a variety of emission scenarios for atmospheric greenhouse gasses and aerosols (e.g., Bueh et al., 2003; Gao et al., 2003; Xu et al., 2003a; Xu et al., 2003b; Jiang et al., 2004a). In contrast, relatively less attention has been paid to the potential impacts of projected climate change on vegetation in China.

The climate system is composed of a number of

*Corresponding author: JIANG Dabang, jiangdb@mail.iap.ac.cn

subsystems. Climate change due to continually increasing atmospheric greenhouse gasses and aerosols inevitably affect these subsystems. It has been amply documented that vegetation is closely related to climate conditions (e.g., Bigelow et al., 2003; Harrison and Prentice, 2003), particularly surface temperature, precipitation, and total cloud amount. Therefore, the joint effects of anthropogenic climate and atmospheric CO_2 concentration changes are likely to modify surface vegetation growth to a lesser or greater extent. In interior China, plant phenology data have revealed that the phenophases of plants have changed greatly alongside surface warming since the 1960s (Zheng et al, 2002), and climate belts during the 1990s generally shifted northward relative to those in the 1950s (Ye et al., 2003). The above evidence confirms that the geographical distribution of vegetation has changed in response to shifts in climate belts, which themselves are closely associated with climate change due to human activities. It is true that large uncertainties exist when climate system models are used to predict spatiotemporal patterns and amplitudes of global warming in the near future. However, it is now commonly accepted that global emissions of greenhouse gasses will lead to a continued and strengthened warming in the 21st century. According to the full range of 35 emission scenarios, a number of climate models have been used to make projections of climate change over the 21st century, and globally-averaged surface temperature is projected to rise by 1.4°C–5.8°C over the period 1990–2100 (Cubasch et al., 2001). In the meantime, similar or slightly stronger surface warming is projected in inland China during this period. Therefore, anthropogenic climate change will inevitably, to a certain extent, impact upon the geographical distribution of vegetation in China in the near future.

Today, the physically-based biome model has become a key tool for exploring past and present vegetation change (e.g., Kutzbach et al., 1998; Lucht et al., 2002; Wang, 2002). Logically, therefore, it could also be used to investigate future vegetation change. Previously, Kaplan et al. (2003) used the BIOME4 model to predict changes in Arctic ecosystems for the 21st century. The model was driven by both atmospheric CO_2 concentration and a transient ocean-atmosphere simulation including sulfate aerosol effects, and the results suggested a potential for large changes in ecosystems north of 55°N. In particular, based on the second Hadley Centre coupled ocean-atmosphere GCM (HadCM2) outputs, as derived from increasing atmospheric greenhouse gasses and sulfate aerosols, Zhao et al. (2002) employed the improved Mapped Atmosphere-Plant-Soil System model to simulate future vegetation in China and found that vegetation change was noticeable, particularly a northward shift of forest boundaries in eastern China. Chen et al. (2003) utilized an aggregated Holdridge Life Zone System to examine the possible response of life zones in China under doubled atmospheric CO_2 concentration, with the input climate elements from the NCAR second-generational regional climate model (RegCM2; Giorgi et al. (1993) nested one way within a global coupled ocean-atmosphere model. It was shown that the responses of different life zones in inland China to the projected climate change would be dramatic. Furthermore, Ding (2002) speculated that the surface temperature and precipitation changes as projected by a number of climate models will significantly modify ecosystems in western China during the 21st century. As such, it is particularly interesting now to employ a relatively reliable biome model to investigate trends of potential vegetation change in China. The results would be helpful for assessing regional environment conditions in the near future.

As a further attempt to explore potential vegetation change in China, the outputs of seven global coupled ocean-atmosphere models under the Special Report on Emission Scenarios (SRES; Nakićenović et al., 2000) A2 and B2 scenarios for atmospheric greenhouse gasses and aerosols are collected from the IPCC Data Distribution Centre. Their abilities to reproduce East Asian monthly surface temperature and precipitation climatologies during 1961–1990 are then evaluated quantitatively. The seven-model ensemble data, together with appropriate atmospheric CO_2 concentration data, are subsequently utilized to drive a biome model. Finally, the projected trends of potential vegetation change during the 2050s and 2090s as compared to 1961–1990 are addressed qualitatively. In this study, the core improvement over previous experiments (e.g., Ni et al., 2000; Zhao et al., 2002; Chen et al., 2003) is the use of a relatively more reliable seven-model ensemble projection under the relatively more representative SRES A2 and B2 scenarios, instead of individual coupled ocean-atmosphere model projection as derived from a simple doubled atmospheric CO_2 level scenario. In addition, ten equilibrium and sensitivity experiments are also conducted to investigate both the attribution and uncertainty of the projected changes in potential vegetation under the SRES A2 scenario during the 2090s.

2. Biome model, climate model data and experimental design

The equilibrium terrestrial biosphere model BIOME3 used here relies on ecophysiological constraints, resource availability, and competition among

plant functional types to simulate potential vegetation and net primary production. BIOME3 has a horizontal grid resolution of 0.5° by 0.5°. The model inputs include atmospheric CO_2 concentration, latitude, soil texture, and monthly climate variables, i.e. surface temperature, precipitation, and sunshine. The model outputs involve 18 kinds of biome types. BIOME3 is suitable for predicting responses of vegetation to climate change alone, as well as both climate change and atmospheric CO_2 enrichment together, and has on the whole been proven to be reliable for the present global map of vegetation. For BIOME3's ability to reproduce the present features of biome distribution and related information in detail, please refer to Haxeltine and Prentice (1996). Previously, Ni (2000) employed the model to simulate the present spatial pattern of potential vegetation and annual net primary production in inland China and showed that, in general, the results were in good agreement with natural vegetation distribution. BIOME3 is therefore regarded as reliable when applied to inland China. The model was also used to simulate potential biomes over the Tibetan Plateau and their responses to global climate change during 2070–2099, as projected by the Hadley Centre ocean-atmosphere model (Mitchell et al., 1995), including the effects of both atmospheric greenhouse gasses and sulfate aerosols. It was found that all vegetation zones over the plateau generally shift northwestward (Ni, 2000). In addition, Jiang et al. (2004b) utilized BIOME3 to reproduce potential vegetation distribution in China at the Last Glacial Maximum and obtained generally sparser-than-present vegetation conditions, qualitatively consistent with proxy evidence.

The monthly climate data used to drive BIOME3 are obtained from the IPCC Data Distribution Centre. They include the outputs of seven global coupled ocean-atmosphere models as run under the SRES A2 and B2 scenarios. It should be noted that the joint radiation forcings of atmospheric greenhouse gasses and aerosols are both derived from observation prior to 2000 and then projected under the SRES A2 and B2 scenarios after that year. For more detail about the model dataset and an overview of each of the seven models (namely CCSR, CGCM2, CSIRO, EH4OPYC3, GFDL, HadCM3, and NCAR-PCM), please visit http://cera-www.dkrz.de/IPCC_DDC/index.html. Incidentally, there are a variety of emission scenarios for atmospheric greenhouse gasses and aerosols according to different world development patterns. The SRES A2 and B2 scenarios chosen in this study are, at present, relatively representative. As a whole, the former (latter) depicts a higher (lower) emission scenario (Nakićenović et al., 2000).

A series of equilibrium experiments have been performed in this investigation, including the control run, B2-50, B2-90, A2-50, A2-90, and sensitivity experiments. The detailed designs for each of these experiments are summarized in Table 1. Here, the control run is used to reproduce present potential vegetation distribution, whereas the other experiments are employed to simulate potential vegetation change in response to the effects of atmospheric CO_2 concentration and/or climate change as projected under the SRES A2 and B2 scenarios during the 2050s and 2090s, respectively. In the control run, the monthly surface temperature, precipitation, and percentage of possible sunshine hours are from the BIOME3 original data package [an improved version of the climate database described by Leemans and Cramer (1991)], and atmospheric CO_2 concentration is set as 331 ppmv, representing an observational average during 1961–1990. In the other experiments, the seven-model ensemble projection products are used. Firstly, the differences in monthly surface temperature and/or precipitation during the 2050s and 2090s relative to 1961–1990 are calculated under the SRES A2 and B2 scenarios for each of the seven models. Then, according to the two different decades and two scenarios, the differences in the seven models are arithmetically averaged when interpolated into a uniform horizontal grid resolution. The above four seven-model ensemble differences are subsequently added to the BIOME3 original climate data. In addition, atmospheric CO_2 concentration during the 2050s and 2090s is taken from the SRES A2 and B2 scenarios (Nakićenović et al., 2000). Other external and internal conditions involved in the BIOME3 configuration remain unchanged.

3. Evaluation of climate model data in East Asia

When attempting to employ the outputs of the seven models to address climate issues in inland China, a key question is to what extent the models can reproduce the present geographical distribution of monthly surface temperature and precipitation in East Asian domain. This bears directly on the credibility of related results as derived from the data of these models.

The seven climate models were driven by the joint radiation forcings of observed annul atmospheric greenhouse gasses and aerosols during 1961–1990. Accordingly, the climate data used to assess model performance involved observed monthly terrestrial surface temperature and precipitation climatologies throughout 1961–1990, taken from the Climatic Research Unit of the University of East Anglia in the United King-

Table 1. Experimental design.

Experiments	Elements		
	Monthly surface temperature (°C)	Monthly precipitation (mm)	Atmospheric CO_2 concentration (ppmv)
Control run	The present		331 (observational average during 1961–1990)
B2-50	The present added by the seven-model ensemble differences during 2051–2060 against 1961–1990 under the SRES B2 scenario		489 (SRES B2 scenario during 2051–2060)
B2-90	Same as B2-50, but replacing 2051–2060 by 2091–2100		591 (SRES B2 scenario during 2091–2100)
A2-50	Same as B2-50, but replacing B2 by A2		551 (SRES A2 scenario during 2051–2060)
A2-90	Same as B2-90, but replacing B2 by A2		783 (SRES A2 scenario during 2091–2100)
A2-90-CO_2	The present	The present	783
A2-90-Tas	A2-90 scenario	The present	331
A2-90-Prec	The present	A2-90 scenario	331

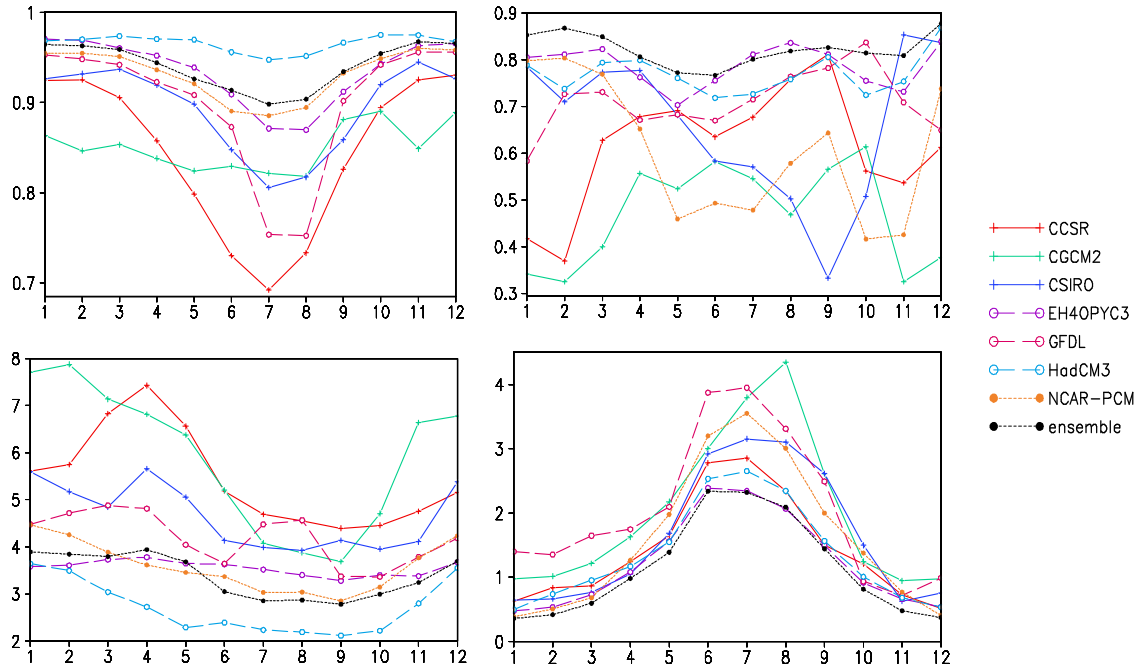

Fig. 1. Monthly spatial correlation coefficient (top-left: surface temperature; top-right: precipitation) and root mean square error excluding systematic model error (lower-left: surface temperature in °C; lower-right: precipitation in mm d^{-1}) between simulated (the seven models and the seven-model ensemble) and observed monthly climatologies in East Asia during 1961–1990. Abscissa denotes month.

dom (New et al., 1999). Here, the spatial correlation coefficient and root mean square error excluding systematic model errors are employed to quantitatively evaluate the simulated East Asian climatologies within the region 18°–54°N, 73°–135°E (dashed rectangular domain in Fig. 2). In general, the former can denote the similarity of geographical distribution between simulation and observation, and the latter can measure the magnitude of intrinsic model errors (Jiang et al., 2005). Figure 1 shows that, although simulation biases exist to a certain extent, the seven models are generally reliable in reproducing both the magnitude and spatial pattern of monthly surface temperature and precipitation in East Asia. On the whole, the performances of the seven models vary from month to month, with relatively better scores during winter months, but with large discrepancies between the models. Comparatively, the ability of the seven models to reproduce precipitation is relatively poor. In addition, the seven-model ensemble produces a relatively larger spatial correlation coefficient and a smaller simulation error than any individual model. The ensemble

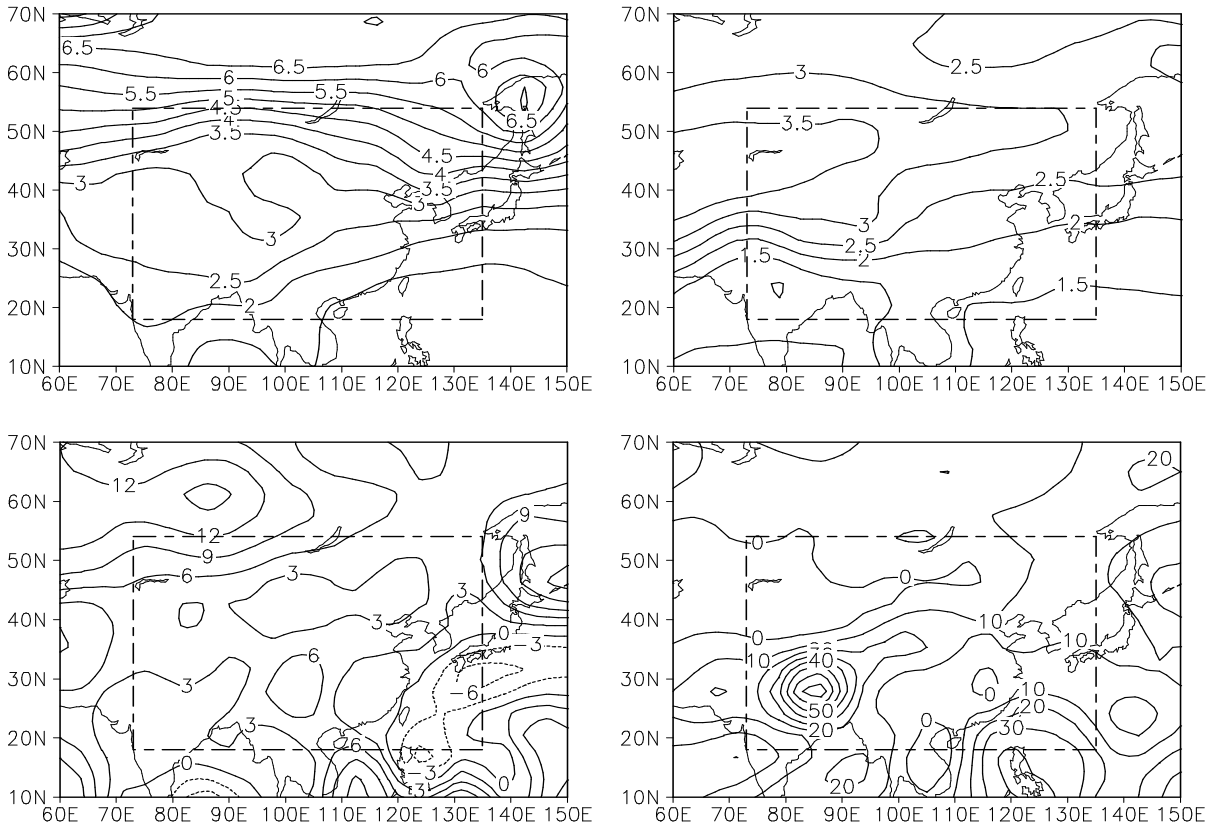

Fig. 2. Differences in surface temperature and precipitation climatologies between 2051–2060 and 1961–1990, as projected by the seven-model ensemble under the SRES A2 scenario. Top-left (top-right) denotes surface temperature in January (July) (°C); and lower-left (lower-right) denotes precipitation in January (July) (mm).

monthly data are consequently more reliable, consistent with a previous investigation focusing on annual and seasonal surface temperature and precipitation (Jiang et al., 2005). As such, it should be reasonable to use the above seven-model ensemble projections to explore future potential vegetation change in China.

4. Projected East Asian climate change

Although the outputs of the seven models have been used to address East Asian climate change in the 21st century (e.g., Jiang et al., 2004a), projected climate scenarios in China for the 2050s and 2090s have not yet been investigated so far. Therefore, January and July surface temperature and precipitation under the SRES A2 scenario in the above two decades are specifically looked at here. Figure 2 shows that surface temperature rises by 1°C–6°C during the 2050s relative to 1961–1990, and the isoline of surface warming amplitude generally distributes zonally and enlarges northward. Moreover, the warming is stronger in January than July, especially at high latitudes. Meanwhile, precipitation increases slightly, but more so in July than January. In July, precipitation enhances notably over the Tibetan Plateau, with a maximum of about 60 mm. Generally, the features of synchronous surface temperature and precipitation changes under the SRES B2 scenario are similar to the above. Of significant difference, however, is weaker surface warming under the SRES B2 scenario, particularly at high latitudes in East Asian domain (figures omitted).

With the steady increasing atmospheric greenhouse gasses and aerosols under the SRES A2 scenario, the spatial pattern of surface warming during the 2090s is consistent with that for the 2050s, and the warming is also much stronger in January than July. However, the warming intensifies notably during the 2090s, with surface temperature augmentation by an average of 3°C–9°C. Meanwhile, the geographical distribution of January precipitation during the 2090s remains similar to that during 1961–1990. On the contrary, July precipitation increases significantly in inland China, especially over the central and eastern Tibetan Plateau, with a maximum monthly augmentation of 130 mm (Fig. 3). Quantitative comparisons reveal that the geographical distribution of monthly

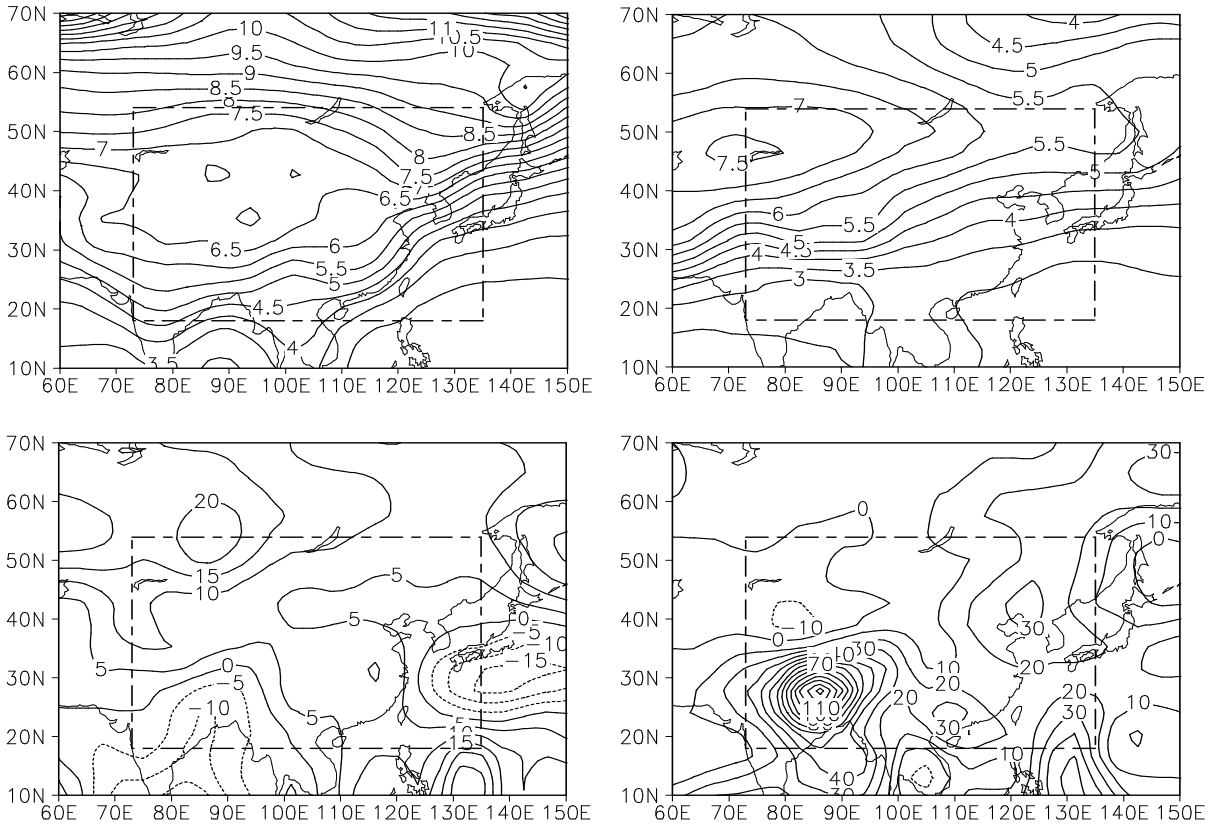

Fig. 3. Differences in surface temperature and precipitation climatologies between 2091–2100 and 1961–1990, as projected by the seven-model ensemble under the SRES A2 scenario. Top-left (top-right) denotes surface temperature in January (July) (°C); and lower-left (lower-right) denotes precipitation in January (July) (mm).

surface temperature and precipitation during the 2090s under the SRES B2 scenario are generally congruent with those under the SRES A2 scenario, except for relatively weaker surface warming (figures omitted).

Additionally, further analyses focusing on the other ten months indicate that under the SRES A2 scenario the spatial pattern of surface warming varies slightly with the months, with a generally larger amplitude at high latitudes in China. Comparatively, the warming is stronger during winter months. Meanwhile, monthly precipitation generally increases during the 2050s and 2090s against 1961–1990. The geographical distribution of precipitation change varies greatly among the months. Overall, precipitation alters slightly during the winter months but increases notably over the Tibetan Plateau during the summer months. Based on the above, it can be concluded that monthly surface temperature and precipitation changes during the 2050s and 2090s relative to 1961–1990, as projected by the seven models under the SRES A2 and B2 scenarios, are huge, especially for surface temperature.

5. Simulated potential vegetation change in China

According to the control run performed by BIOME3 (Fig. 4), the geographical distribution of potential vegetation in China is characterized jointly by temperate broadleaved evergreen forest in South China and the mid-upper reaches of the Yangtze River valley; temperate deciduous forest in the Huanghe River and Huaihe River regions and the middle and lower reaches of the Yangtze River valley; temperate mixed forest in Shaanxi, Henan, and southern Gansu Provinces; moist savannas and temperate deciduous forest, as well as temperate mixed forest, in North China; temperate mixed forest in mid-eastern Northeast China; evergreen forest/woodland in northern Northeast China; short grassland in mid-eastern Inner Mongolia; arid shrubland/steppe in western Inner Mongolia; alpine tundra over the Tibetan Plateau; arid shrubland/steppe in the northern Uygur Autonomous Region of Xinjiang; and desert and arid shrubland/steppe in the southern Uygur Autonomous Region of Xinjiang. Qualitative comparisons indicate

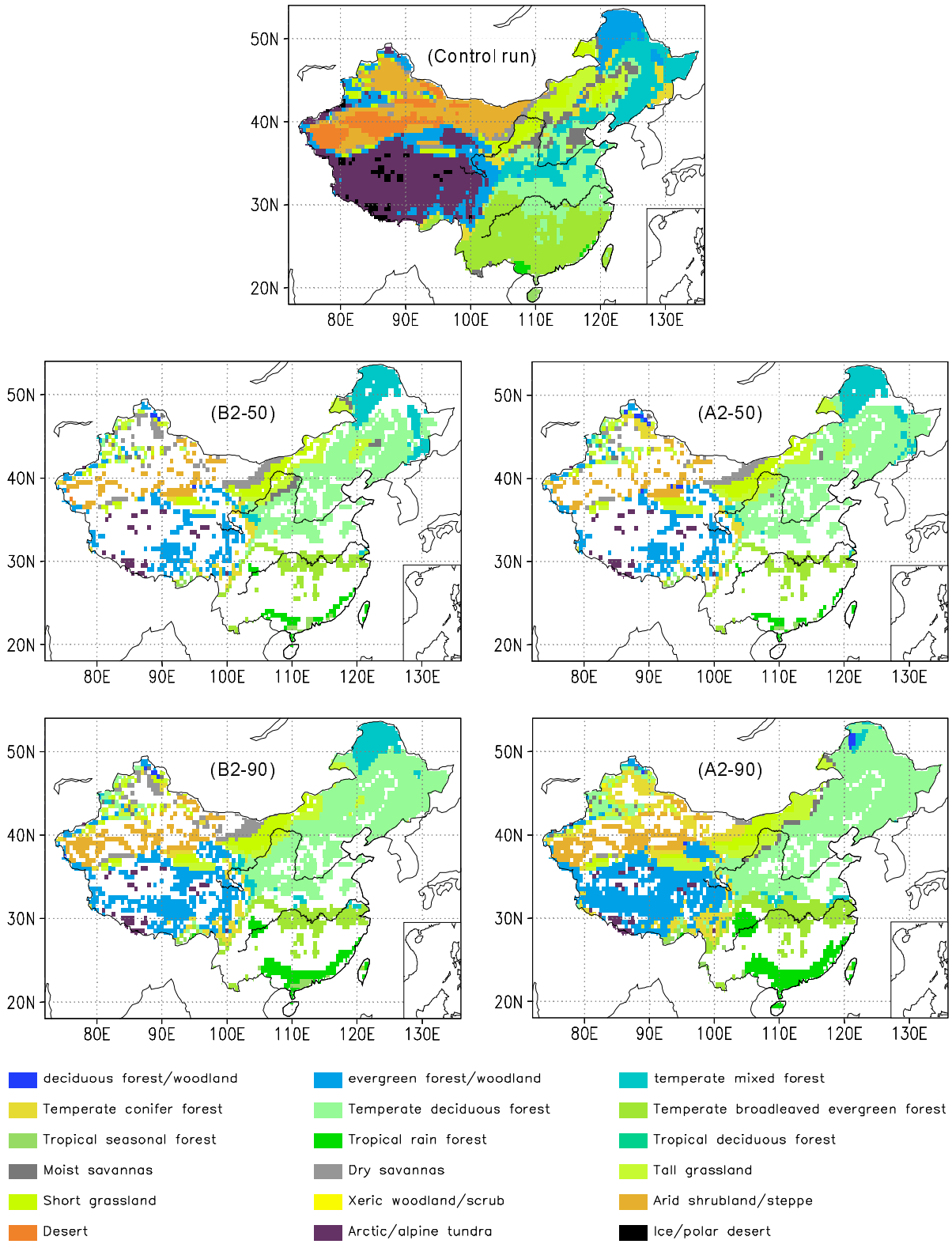

Fig. 4. Potential vegetation distribution in the control run, and the differences of potential vegetation in the experiments B2-50, B2-90, A2-50, and A2-90 relative to the control run (blank grid denotes no vegetation differences in the four experiments against the control run).

that although climate and soil texture data are different, the geographical distribution of potential vegetation in the control run agrees well with the present potential vegetation map (Ni et al., 2000, Fig. 1b) and generally agrees with the nature vegetation map of China (Ni et al., 2000, Fig. 1a).

The experiments B2-50, B2-90, A2-50, and A2-90 reveal that the geographical distribution of potential vegetation in China alters greatly during the 2050s and 2090s relative to the control run (Fig. 4). In the B2-50 experiment, the potential vegetation pattern differs from the control run in the following main ways (control run vegetation type in parentheses): tropical rainforest and tropical seasonal forest (temperate broadleaved evergreen forest) in coastal South China; temperate broadleaved evergreen forest (temperate deciduous forest) in the middle and lower reaches of the Yangtze River valley; temperate deciduous forest (temperate mixed forest) in much of Shaanxi and Henan Provinces; temperate deciduous forest (temperate mixed forest) in North China and mid-southern Northeast China; temperate mixed forest (evergreen forest/woodland) in northern Northeast China; tall grassland (short grassland) in eastern Inner Mongolia; short grassland and dry savannas (arid shrubland/steppe) in central Inner Mongolia; and evergreen forest/woodland (alpine tundra) over the southwestern Tibetan Plateau.

Overall, the spatial pattern of potential vegetation is similar between the A2-50 and B2-50 experiments. Both are signified by a significant northward shift of potential vegetation belts in eastern China relative to the control run. However, potential vegetation change against the control run is more extensive in the A2-50 than the B2-50 experiment. For instance, a larger range of temperate deciduous forest in mid-northern Northeast China, short grassland in mid-eastern Inner Mongolia, and evergreen forest/woodland over the southwestern Tibetan Plateau are present in the A2-50 experiment.

The range of potential vegetation change extends during the 2090s relative to the 2050s, almost covering the whole Chinese mainland relative to the control run. In the B2-90 experiment, potential vegetation change that differs significantly from the control run can be summarized by the following (control run vegetation type in parentheses): tropical rainforest and tropical seasonal forest (temperate broadleaved evergreen forest) in South China; temperate broadleaved evergreen forest (temperate deciduous forest) in the middle and lower reaches of the Yangtze River valley; tropical rainforest (temperate broadleaved evergreen forest) in southwestern Sichuan Province, temperate deciduous forest (short grassland) in the Hetao region, temperate deciduous forest (temperate mixed forest) in the southwest of the Hetao region; temperate deciduous forest (moist savannas, temperate mixed forest, and short grassland) in North China and most parts of central and southern Northeast China; temperate mixed forest (evergreen forest/woodland) in northern Northeast China; dry savannas and short grassland (arid shrubland/steppe) in central Inner Mongolia; tall grassland (short grassland) and temperate deciduous forest (tall grassland and moist savannas) in mid-eastern Inner Mongolia; and evergreen forest/woodland (alpine tundra) over the mid-southern Tibetan Plateau, which is linked to increasing summer precipitation during the 2090s as projected by the seven-model ensemble. In addition, a large range of desert in the Hui Autonomous Region of Ningxia, Qinghai Province, and the mid-southern area of the Uygur Autonomous Region of Xinjiang in the control run is replaced by arid shrubland/steppe in the B2-90 experiment, which is without doubt beneficial to the improvement of the environment in western China.

In the A2-90 experiment, the geographical distribution of potential vegetation change relative to the control run is generally consistent with the B2-90 experiment, but with more extensive areas. It is found that potential vegetation change occurs across almost the whole of the Chinese mainland, apart from in central South China and the lower reaches of the Changjiang River–Huaihe River. Significant differences compared to the B2-90 experiment are characterized by: extended temperate broadleaved evergreen forest in the middle and lower reaches of the Yangtze River valley; tropical rainforest in the mid-eastern Sichuan Basin; temperate deciduous forest instead of temperate mixed forest in the B2-90 experiment in northern Northeast China; evergreen forest/woodland in Tibet and western Sichuan Province; and arid shrubland/steppe in the Hui Autonomous Region of Ningxia, Qinghai Province, and in the mid-southern area of the Uygur Autonomous Region of Xinjiang.

It is usually recognized that multi-model ensemble products are most reliable when a number of climate models are used to project future climate change due to anthropogenic factors (IPCC, 2001). Accordingly, the above scenarios of potential vegetation change generally denote an average behavior of BIOME3's response to the projections of the seven models. Actually, exploring the uncertainty of potential vegetation change remains of parallel importance. As a further investigation, therefore, seven equilibrium experiments are additionally conducted here, keeping the experimental design the same as in the A2-90 experiment, except for driving BIOME3 with the difference projected by each of the seven models respectively, instead

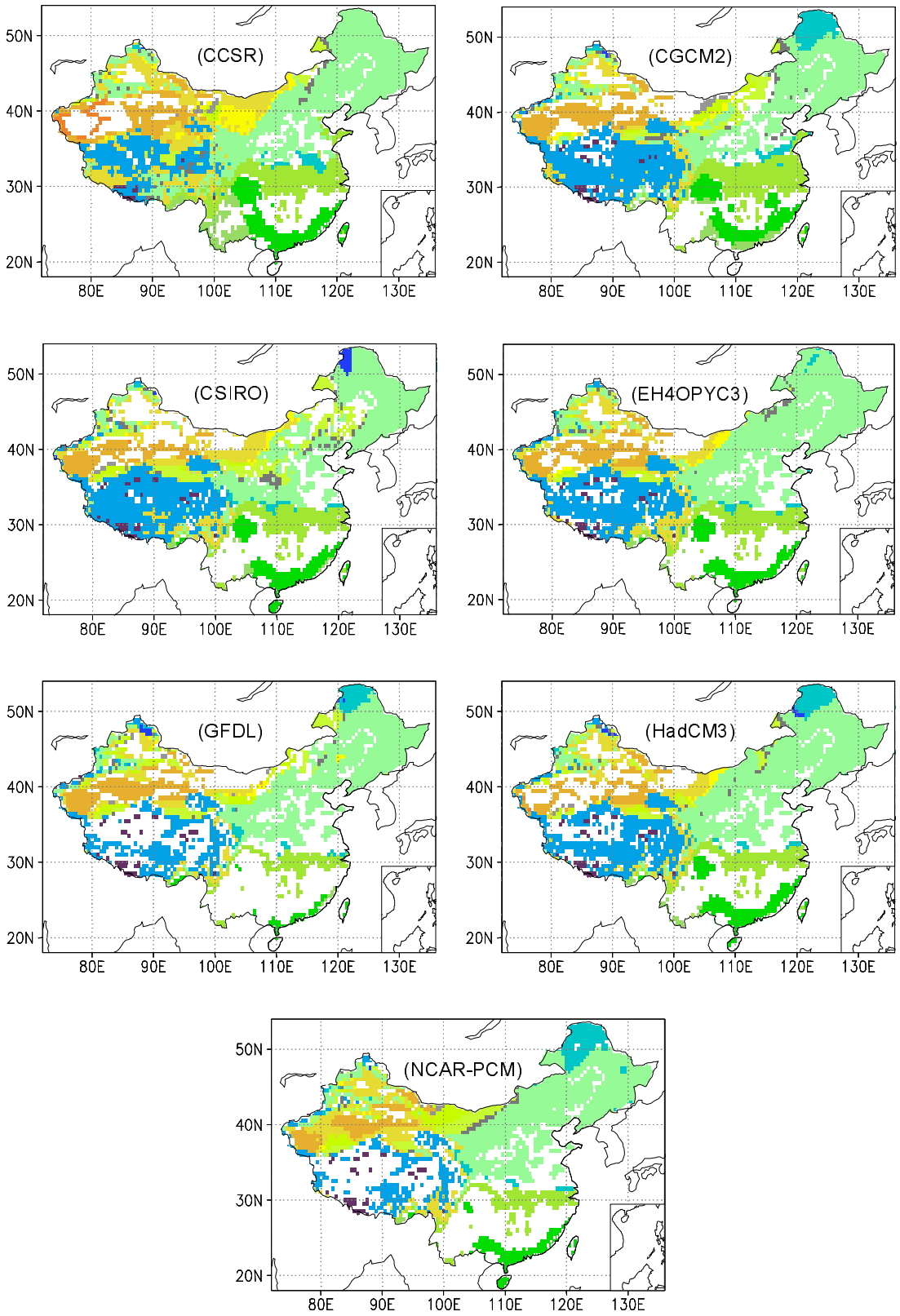

Fig. 5. Differences in potential vegetation distribution during the 2090s, as projected by each of the seven models under the SRES A2 scenario relative to the control run displayed in Fig. 4 (vegetation-color translation is the same as in Fig. 4, and a blank grid denotes no vegetation differences against the control run).

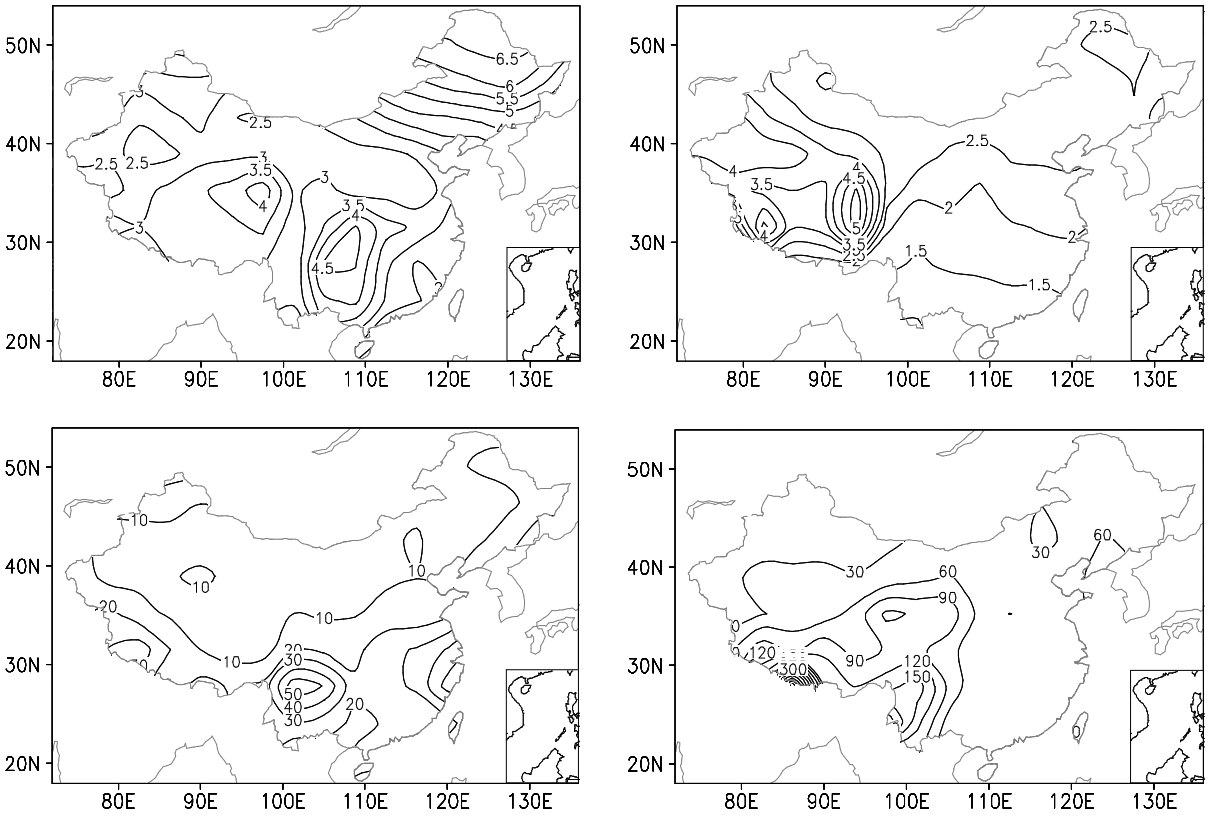

Fig. 6. The root mean square between pairs of the seven models (MRMS): the upper denotes surface temperature in °C, and the lower denotes precipitation in mm (left for January and right for July).

of the seven-model ensemble difference. It follows that the geographical distribution of potential vegetation in each of the seven experiments is dramatically different from the control run, implying significant changes in potential vegetation during the 2090s relative to the present (Fig. 5). Moreover, the spatial pattern of potential vegetation change in each of the seven experiments generally remains similar to that in the A2-90 experiment, i.e., potential vegetation belts generally shift northward, particularly in eastern China. This means that the trend of change in potential vegetation on a large scale is qualitatively consistent among the models.

In contrast, the response of BIOME3 to each individual projection also displays different behavior from the A2-90 experiment. For example, the changes in potential vegetation disagree notably in Northeast China and over the Tibetan Plateau among the models. Therefore, uncertainty in potential vegetation change, to a certain extent, also exhibits even if the models are driven by the same atmospheric CO_2 concentration. Actually, this uncertainty can be attributed to the scatter of climate change as projected by the seven models under the SRES A2 scenario. After Pinot et al. (1999), the root mean square between pairs of models (MRMS) is defined here as

$$\mathrm{MRMS} = \sqrt{\frac{\sum_{i=1}^{n}\sum_{j=1}^{n}(x_i - x_j)^2}{m}},$$

with $n = 7$ (number of models) and $m = 21$ (number of pairs of models). The spread of January and July surface temperature and precipitation projections among the seven models is accordingly given in Fig. 6. On the whole, the scatter of surface temperature is relatively larger over the Tibetan Plateau and enlarges northward in East Asia, and the scatter of precipitation is dramatically larger over the Tibetan Plateau, particularly in July, and enlarges southward in East Asia. As such, the projected change of potential vegetation over the Tibetan Plateau should be highly uncertain, which has been shown in Fig. 5.

In an attempt to explore the underlying reasons for the simulated changes in potential vegetation under the SRES A2 scenario during the 2090s, three sensitivity experiments, namely A2-90-CO_2, A2-90-Tas, and A2-90-Prec, were designed (see Table 1 for further de-

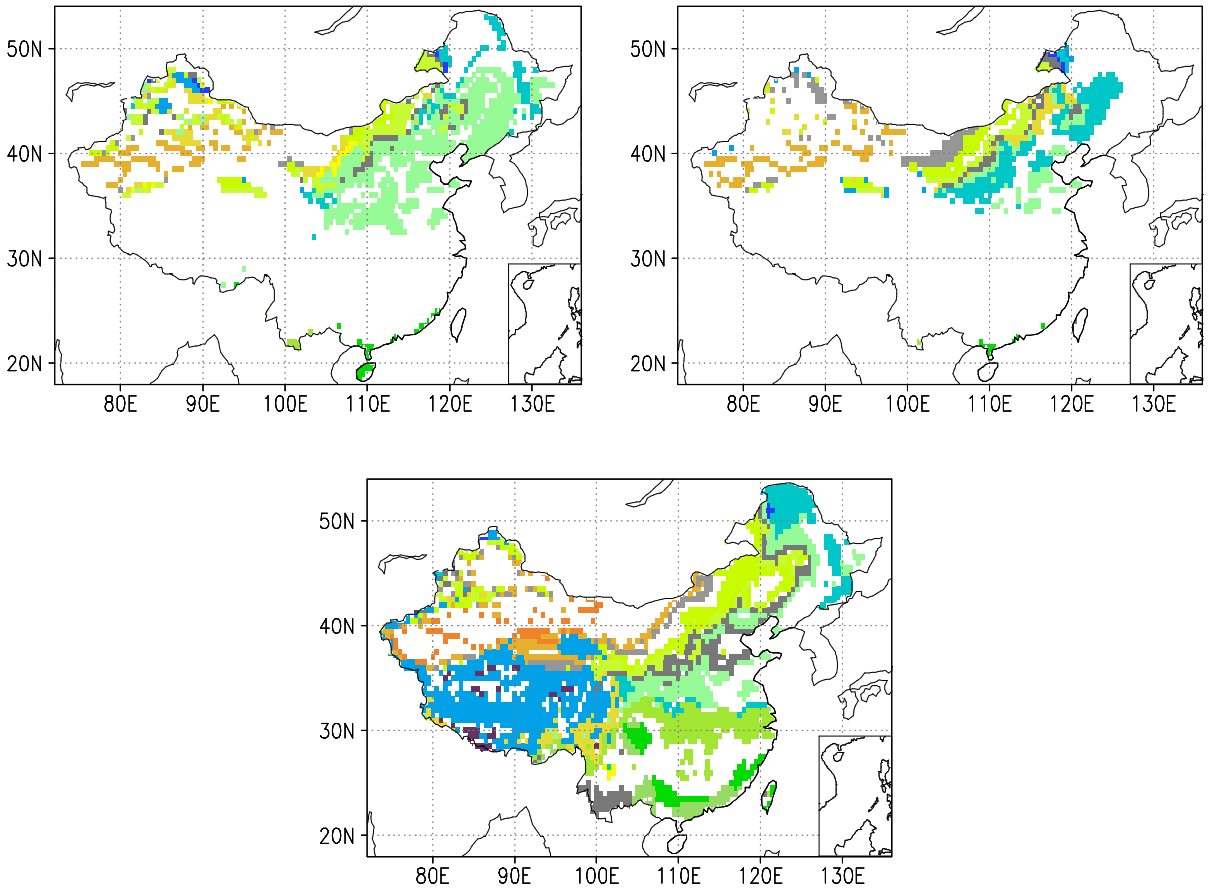

Fig. 7. Atmospheric CO_2 concentration (top-left), the seven-model ensemble precipitation (top-right) and surface temperature (lower) induce changes of potential vegetation distribution under the SRES A2 scenario during the 2090s relative to the control run displayed in Fig. 4 (vegetation-color translation is the same as in Fig. 4, and a blank grid denotes no vegetation differences against the control run).

tails). It is indicated that the change of atmospheric CO_2 concentration itself can induce dramatic changes in potential vegetation north of around 35°N in Chinese mainland (Fig. 7). Of significance is that temperate deciduous forest takes the place of temperate mixed forest and short grassland in much of central China, North China, and Northeast China, and tall grassland replaces arid shrubland/steppe in the northern area of the Uygur Autonomous Region of Xinjiang. The influence of precipitation change on potential vegetation is also noticeable north of around 35°N in Chinese mainland (Fig. 7). For instance, temperate mixed forest takes the place of short grassland in mid-eastern Northeast China, and dry savannas replace arid shrubland/steppe in central Inner Mongolia. It can also be seen that the trends of change relative to the control run (Fig. 4), as respectively derived from atmospheric CO_2 concentration and projected precipitation change, are largely different when they are compared with each other for the same location, such as in mid-eastern Northeast China. Further investigation reveals that the influence of projected surface temperature change on potential vegetation is dominant (Fig. 7). Changes in potential vegetation relative to the control run occur in much of inland China. On the whole, potential vegetation belts shift northward in central and eastern China and change significantly over the Tibetan Plateau. Actually, comparing the results of the experiments A2-90, A2-90-CO_2, A2-90-Prec, and A2-90-Tas with the control run indicates that changes in the spatial pattern of potential vegetation in Chinese mainland, as registered in the A2-90 experiment, are mostly attributable to surface temperature change south of 35°N and to the joint changes of surface temperature, precipitation, and atmospheric CO_2 concentration north of 35°N.

6. Conclusions

The outputs of seven global coupled ocean-atmosphere models, as forced by the SRES A2 and

B2 scenarios for atmospheric greenhouse gasses and aerosols, together with corresponding atmospheric CO_2 concentration, have been jointly used to drive BIOME3 to examine potential vegetation change in China for the 2050s and 2090s. The primary conclusions are as follows:

(1) Potential vegetation belts shift northward notably in central and eastern China, whereas they change only slightly in western China during the 2050s relative to 1961–1990, although noticeable changes are registered in most parts of the Uygur Autonomous Region of Xinjiang and in western Tibet.

(2) During the 2090s, the trend of change in potential vegetation is generally consistent with that during the 2050s on a large scale. Comparatively, the changes are more extensive during the 2090s, particularly in western China where vegetation tends to become denser.

(3) The response of BIOME3 to each individual model projection under the SRES A2 scenario during the 2090s reveals model-dependent uncertainty of potential vegetation change, which is due to the scatter of projected surface temperature and precipitation changes by the models.

(4) The projected changes in potential vegetation in inland China under the SRES A2 scenario during the 2090s are attributable to surface temperature changes south of 35°N and to the joint changes of surface temperature, precipitation, and atmospheric CO_2 concentration north of 35°N.

As an agricultural country, climate change affects food supplies in the Chinese society and essentially acts a key factor in the formation of regional environmental conditions. Therefore, exploring potential vegetation change due to anthropogenic climate change remains interesting. Although large uncertainties exist when climate models are used to project anthropogenic climate change under a variety of emission scenarios for atmospheric greenhouse gases and aerosols, human-induced surface warming over the second half of the 20th century and expected surface warming over the 21st century have been widely reported (IPCC, 2001). The above precondition makes it reasonable to employ the relatively reliable BIOME3 to investigate potential vegetation change in China, particularly when one takes into account that the model can dependably reproduce the geographical distribution of natural vegetation on a global scale (Haxeltine and Prentice, 1996) and in interior China (Ni et al., 2000). As such, the qualitative results obtained in this study should be beneficial to assess potential vegetation and environment change in interior China under continually intensified global warming in the near future.

Acknowledgements. The author thanks the IPCC Data Distribution Center for providing model outputs, Prof. I. Colin Prentice for supplying the BIOME3 model code, Prof. J. Ni for helping to run the model, Dr. Y. Xu for providing atmospheric CO_2 concentration data, and Prof. N. Zeng and an anonymous reviewer for constructive comments on earlier versions of the article. This research was jointly supported by the Chinese Academy of Sciences under Grant No. KZCX3-SW-229 and the National Natural Science Foundation of China under Grant Nos. 40505017 and 40405015.

REFERENCES

Bigelow, N. H., and Coauthors, 2003: Climate change and Arctic ecosystems: 1. Vegetation changes north of 55°N between the last glacial maximum, mid-Holocene, and present. *J. Geophys. Res.*, **108**(D19), 8170, doi:10.1029/2002JD002558.

Bueh, C., U. Cubasch, Y. Lin, and L. Ji, 2003: The change of North China climate in transient simulations using the IPCC SRES A2 and B2 scenarios with a coupled atmosphere-ocean general circulation model. *Adv. Atmos. Sci.*, **20**, 755–766.

Chen, X., X. Zhang, and B. Li, 2003: The possible response of life zones in China under global climate change. *Global and Planetary Change*, **38**, 327–337.

Cubasch, U., and Coauthors, 2001: Projections of the future climate change. *Climate Change 2001: The Scientific Basis*, T. J. Houghton et al., Eds., Cambridge University Press, New York, 525–582.

Ding, Y., 2002: *Prediction of Environment Changes of Western China*. Science Press, Beijing, 231pp. (in Chinese)

Gao, X., Z. Zhao, Y. Ding, R. Huang, and F. Giorgi, 2003: Climate change due to greenhouse effects in China as simulated by a regional climate model, Part II: Climate change. *Acta Meteorologica Sinica*, **61**(1), 29–38. (in Chinese)

Giorgi, F., M. R. Marinucci, and G. T. Bates, 1993: Development of a second-generational regional climate model (RegCM2). Part II: Boundary-layer and radiative transfer processes. *Mon. Wea. Rev.*, **121**, 2794–2813.

Harrison, S. P., and I. C. Prentice, 2003: Climate and CO_2 controls on global vegetation distribution at the last glacial maximum: Analysis based on palaeovegetation data, biome modeling and palaeoclimate simulations. *Global Change Biology*, **9**, 983–1004.

Haxeltine, A., and I. C. Prentice, 1996: BIOME3: An equilibrium terrestrial biosphere model based on ecophysiological constraints, resource availability, and competition among plant functional types. *Global Biogeochemical Cycles*, **10**(4), 693–709.

IPCC, 2001: *Climate Change 2001: The Scientific Basis*. Cambridge University Press, Cambridge, United Kingdom, and New York, USA, 881pp.

Jiang, D., H. Wang, and X. Lang, 2004a: Multimodel en-

semble prediction for climate change trend of China under SRES A2 scenario. *Chinese Journal of Geophysics*, **47**(5), 878–886.

Jiang, D., H. Wang, and X. Lang, 2004b: On the possibility of ice sheet over the Tibetan Plateau at the Last Glacial Maximum. *Chinese J. Atmos. Sci.*, **28**(1), 28–34.

Jiang, D., H. Wang, and X. Lang, 2005: Evaluation of East Asian climatology as simulated by seven coupled models. *Adv. Atmos. Sci.*, **22**(4), 479–495.

Kaplan, J. O., and Coauthors, 2003: Climate change and Arctic ecosystems: 2. Modeling, paleodata-model comparisons, and future projections. *J. Geophys. Res.*, **108**(D19), 8171, doi:10.1029/2002JD002559.

Kutzbach, J., R. Gallimore, S. Harrison, P. Behling, R. Selin, and F. Laarif, 1998: Climate and biome simulations for the past 21,000 years. *Quaternary Science Reviews*, **17**, 473–506.

Leemans, R., and W. Cramer, 1991: The IIASA climate database for mean monthly values of temperature, precipitation and cloudiness on a terrestrial grid. RR-91-18, International Institute for Applied Systems Analysis, Laxenburg.

Lucht, W, and Coauthors, 2002: Climatic control of the high-latitude vegetation greening trend and Pinatubo effect. *Science*, **296**, 1687–1689.

Mitchell, J. F. B., T. C. Johns, J. M. Gregory, and S. F. B. Tett, 1995: Climate response to increasing levels of greenhouse gases and sulphate aerosols. *Nature*, **376**, 501–504.

Nakićenović, N., and Coauthors, 2000: *IPCC Special Report on Emissions Scenarios*. Cambridge University Press, Cambridge, UK, 599pp.

New, M., M. Hulme, and P. D. Jones, 1999: Representing twentieth century space-time climate variability. Part I: Development of a 1961–90 mean monthly terrestrial climatology. *J. Climate*, **12**, 829–856.

Ni, J., 2000: A simulation of biomes on the Tibetan Plateau and their responses to global climate change. *Mountain Research and Development*, **20**(1), 80–89.

Ni, J., M. T. Sykes, I. C. Prentice, and W. Cramer, 2000: Modelling the vegetation of China using the process-based equilibrium terrestrial biosphere model BIOME3. *Global Ecology and Biogeography*, **9**, 463–479.

Pinot, S., G. Ramstein, S. P. Harrison, I. C. Prentice, J. Guiot, M. Stute, and S. Joussaume, 1999: Tropical paleoclimates at the Last Glacial Maximum: Comparison of Paleoclimate Modeling Intercomparison Project (PMIP) simulations and paleodata. *Climate Dyn.*, **15**, 857–874.

Qin, D., 2003: Facts, impact, adaptation and mitigation strategy of climate change. *Chinese Science Foundation*, 1–3. (in Chinese)

Wang, H., 2002: The mid-Holocene climate simulated by a grid-point AGCM coupled with a biome model. *Adv. Atmos. Sci.*, **19**(2), 205–218.

Xu, Y., Y. Ding, Z. Zhao, and J. Zhang, 2003a: A scenario of seasonal climate change of the 21st century in Northwest China. *Climatic and Environmental Research*, **8**(1), 19–25. (in Chinese)

Xu, Y., F. Xue, and Y. Lin, 2003b: Changes of surface air temperature and precipitation in China during the 21st century simulated by HadCM2 under different greenhouse gas emission scenarios. *Climatic and Environmental Research*, **8**(2), 209–217. (in Chinese)

Ye, D., Y. Jiang, and W. Dong, 2003: The northward shift of climatic belts in China during the last 50 years and the corresponding seasonal responses. *Adv. Atmos. Sci.*, **20**(6), 959–967.

Zhao, M., R. P. Neilson, X. Yan, and W. Dong, 2002: Modelling the vegetation of China under changing climate. *Acta Geographica Sinica*, **57**(1), 28–38. (in Chinese)

Zheng, J., Q. Ge, and Z. Hao, 2002: Impacts of climate warming on plants phenophases in China for the last 40 years. *Chinese Science Bulletin*, **47**(21), 1826–1831.